IEEE Access
Multidisciplinary ⋮ Rapid Review ⋮ Open Access Journal

Received October 26, 2019, accepted November 19, 2019, date of publication November 22, 2019,
date of current version December 6, 2019.

Digital Object Identifier 10.1109/ACCESS.2019.2955104

A New Design of Filtering Power Dividers With Arbitrary Constant Phase Difference, Impedance Transformation, and Good Isolation

YUN-PENG LYU[1], (Member, IEEE), LEI ZHU[2], (Fellow, IEEE), AND CHONG-HU CHENG[1], (Member, IEEE)

[1]College of Telecommunications and Information Engineering, Nanjing University of Posts and Telecommunications, Nanjing 210003, China
[2]Department of Electrical and Computer Engineering, Faculty of Science and Technology, University of Macau, Zhuhai 999078, China

Corresponding authors: Lei Zhu (leizhu@umac.mo) and Chong-Hu Cheng (chengch@njupt.edu.cn)

This work was supported in part by the National Natural Science Foundation of China under Grant 61901226, in part by the Natural Science Foundation of Jiangsu Province under Grant BK20190727, in part by the Universities Natural Science Research General Project under Grant 19KJB510045, in part by the Nanjing University of Posts and Telecommunications Scientific Foundation under Grant NY219128, and in part by the Multi-Year Research Grant from the University of Macau under Grant MYRG2018-00073-FST.

ABSTRACT This paper proposes a new class of filtering power dividers integrated with phase shifter and impedance transformer simultaneously for the first time. In contrast to the conventional approaches, the proposed filtering power dividers consist of two asymmetrical generalized bandpass networks, that can achieve arbitrary constant phase difference and good isolation at two output ports. On the one hand, the magnitude and phase properties of two generalized n^{th}-order bandpass networks are systematically studied and fully considered to realize the prescribed power division, filtering function, constant phase difference, and impedance transformation in the co-design. On the other hand, in order to obtain good isolation, the resonator's type and impedance of these two asymmetrical networks are carefully considered and closed-form formula of isolation resistor is also deduced. Theoretical results show that the proposed topology can achieve perfect isolation over entire passband for the arbitrary phase difference. Meanwhile, the synthesis procedures are presented for a quick design process. Finally, two porotypes (90° power divider and 120° power divider) with specified different operation bandwidth (15% and 25%), filter order (3rd and 6th), and terminated port impedances (50Ω and 100Ω) are synthesized, fabricated, and tested to verify the proposed design method and predicted frequency responses. It firstly integrates the power divider, filter, phase shifter, and impedance transformer into single component and has several additional advantages, such as low cost, simple geometry, small phase deviation and amplitude imbalance, and easiness for design and fabrication.

INDEX TERMS Filtering power divider, arbitrary constant phase difference, good isolation, asymmetrical networks, synthesis design.

I. INTRODUCTION

In modern wireless and mobile communication systems, a RF/microwave transceiver is usually constructed by various components, including the filters, power dividers (PDs), phase shifters, antennas, and so on. At the low gigahertz frequency region, these passive components usually occupy an excessive area apiece. To reduce the fabrication cost and provide system miniaturization, multifunctional microwave components have aroused great research interests [1]–[5].

The associate editor coordinating the review of this manuscript and approving it for publication was Wenjie Feng.

Among them, filtering power dividers (FPD) is a typical multi-functional component which possess both frequency selectivity and power division/combination. In recent years, many efforts have been made to develop diverse integrated methods. One of the most popular approaches is to replace quarter-wave (λ/4) transmission lines in Wilkinson power dividers with the different filtering structures. The four 0° feeding coupling resonators [6], dual-mode resonators [7], stepped-impedance ratio multimode resonators (SIR-MMRs) [8], and transversal filtering structures [9] are embedded to achieve two-pole singe-/dual-/tripe-/quad-passband FPDs. To achieve high-order filtering response with

steep reject-ion skirt, multi-stage in-line and cross-coupling topology is developed [10], [11]. Besides, the coupled-lines can be also utilized to replace the quarter-wavelength transmission line, which can obtain wideband response [12], [13]. Moreover, the isolation is another important design index for the FPDs. In order to realize good isolation with high isolation-level and extended bandwidth, the special coupling topology [14], distributed isolation network [15], and stepped-impedance resonator network [16] are studied and adopted in the FPDs.

Nowadays, magnitude responses of PDs can be realized in different forms, such as the singe-/dual-/tripe-/quad-band [6]–[9], wideband [12], [13], and different filter-orders [10], [11]. However, the phase responses of PDs usually has only two states, that is, in-phase [6]–[16] and out-of-phase [17]–[19]. Besides these two inherent phase differences (0° and 180°), feature of arbitrary phase difference is indispensable in the plenty of applications. For example, the 90° and 120° PDs are widely used in multi-fed circularly polarized (CP) antennas, power amplifiers, modulators and reflectometers [20]–[24]. In [25], a PD with 5.625°, 11.25°, 22.5°, 45°, 90°, and 180° is presented for the multiphase feeding-network. However, all these reported PDs are designed by cascading additional phase shifters to the conventional Wilkinson PDs, which inevitably increase the circuit size. In summary, they are realized by two individual components.

Recently, the integration of PD and phase shifter into one circuity is getting research attention. In [26], the CVT and CCT technologies are developed to achieve novel PDs with an arbitrary phase difference, but specified phase difference can be only obtained at a single frequency point, restricting them for narrow applications. In [27], the multi-functional phase shifters on multiple resonant technology is presented, which can achieve arbitrary power distribution and constant phase differences at multiple outputs and it is a new kind of PD. In [28], design of complex weighted feeding network is proposed based on the similar working principle. However, the proposed PDs in [27] and [28] don't have the ability of isolation, which inevitably results in the poor matching for output ports and large ripples in the magnitude responses. Meanwhile, the mismatching at outputs will seriously cause large phase deviation and amplitude imbalance. In addition, the ability of impedance transformation is not demonstrated.

In this paper, we propose a new class of filtering power divider which firstly integrates the PD, filter, phase shifter, and impedance transformer into single component as shown in Fig. 1. By fully considering the magnitude and phase properties of two asymmetrical n^{th}-order bandpass networks, the power-division ratio, filtering response, constant phase difference, and impedance transformation can be prescribed simultaneously. What's more, perfect isolation of outputs can be achieved over entire passband theoretically under arbitrary phase difference and terminated impedance for the proposed PD. Closed-form formulas and synthesis method are presented, allowing for a quick design process. Finally,

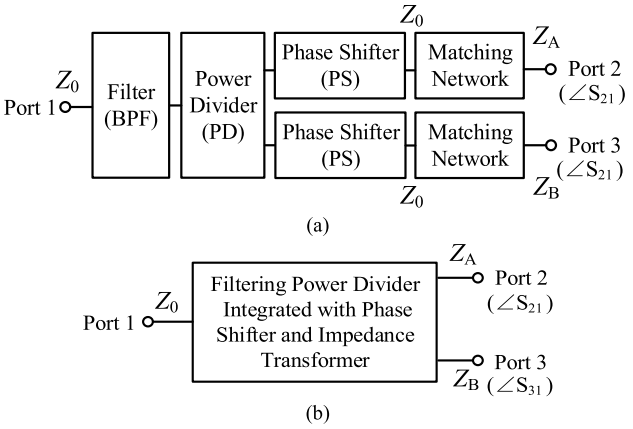

FIGURE 1. Schematics of the two filtering power dividers with arbitrary constant phase difference, impedance transformation, and good isolation. (a) Traditional design with cascaded filter, power divider, phase shifter, and impedance transformer. (b) Proposed design with single component.

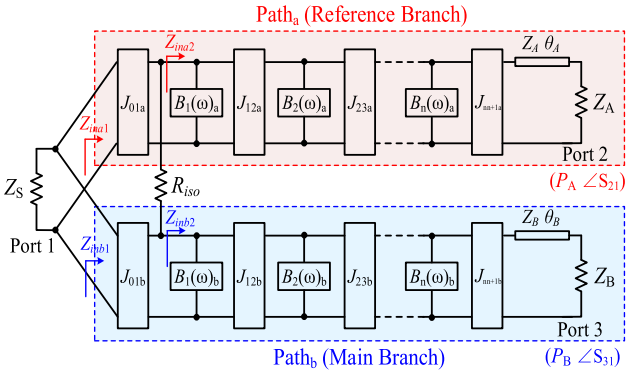

FIGURE 2. Circuit diagram of the proposed filtering power divider with arbitrary constant phase difference, impedance transformation, and good isolation.

two prototypes are designed and fabricated to confirm the design concept and to validate the predicted results.

II. FUNDAMENTAL THEORY

A. CIRCUIT DIAGRAM

Fig. 2 depicts the circuit diagram of the proposed filtering PD with arbitrary constant phase difference. It consists of the two generalized n^{th}-order BPF networks, that is, main and reference branches. Each branch has its own distinctive admittance inverters and susceptances, denoted as J_i, $_{i+1a}/B_i(\omega)_a$ and J_i, $_{i+1b}/B_i(\omega)_b$, respectively, where J_i, $_{i+1a} \neq J_i$, $_{i+1b}$ and $B_i(\omega)_a \neq B_i(\omega)_b$. The terminated impedances of three ports are denoted as Z_S, Z_A, and Z_B, and the isolation resistor is R_{iso}. At two output ports, the markers P_A and P_B indicate the output power, whereas the $\angle S_{21}$ and $\angle S_{31}$ are the output phase shift. For the proposed PD, the power-division ratio is defined as $P_A/P_B = k^2$ and phase difference is defined as $\Delta\Phi = \angle S_{21} - \angle S_{31}$. All these design indexes, including the Z_S, Z_A, Z_B, k^2 and $\Delta\Phi$, can be arbitrarily prescribed in the given synthesis method. Meanwhile, the perfect isolation ($S_{32} = 0$) can be achieved theoretically.

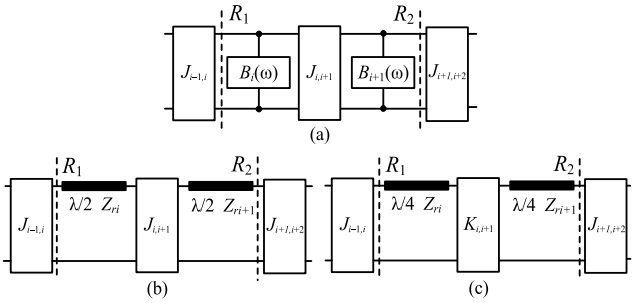

FIGURE 3. Network segments of (a) generalized BPF network. (b) λ/2 resonators and J inverters. (c) λ/4 resonators and alternative J/K inverters.

In addition, the filter order and resonators type can be freely chosen for this proposed FPD. For definiteness and without loss of generality, the cases of λ/2 resonator and λ/4 resonator are both taken into account in this design in Fig. 3. Since the proposed structure is asymmetrical, conventional even-/ odd-mode analysis method for FPD is not applicable. Instead, a new design method based on circuit theory as well as transmission-line theory is carried out and will be illustrated in detail in the following sections.

B. POWER DIVISION AND IMPEDANCE TRANSFORMATION

In order to realize the power-division ratio of k^2 ($P_A/P_B = k^2$), input impedances of Z_{ina1} and Z_{inb1} shown in Fig. 2 are required to satisfy the following conditions

$$\begin{cases} \dfrac{Z_{inb1}}{Z_{ina1}} = k^2 \\ \dfrac{Z_{ina1}Z_{inb1}}{Z_{ina1}+Z_{inb1}} = R_S \end{cases} \tag{1}$$

then the Z_{ina1} and Z_{inb1} can be derived as

$$Z_{ina1} = (1+\frac{1}{k^2})Z_S, \quad Z_{inb1} = (1+k^2)Z_S \tag{2}$$

Meanwhile, another condition for power-division ratio of k^2 is that the ratio of the Z_{inb2} to Z_{ina2} equals to k^2, that is

$$Z_{ina2} = Z_{Ar}, \quad Z_{inb2} = k^2 Z_{Ar} \tag{3}$$

where Z_{Ar} is an arbitrary impedance in design [29].

Fig. 4 depicts the sub-networks of the main and reference branches for the proposed PD. Each branch of the proposed PD has own respective filter order N, bandpass ripple L_{Ar}, and fractional bandwidth (FBW). In this context, the filter order N and bandpass ripple L_{Ar} are set to be identical in the two branches. At the center frequency f_0, the susceptances of these two branches are both equal to zero, such as

$$B_1(\omega_0)_a = B_2(\omega_0)_a = \cdots = B_N(\omega_0)_a = 0 \tag{4a}$$
$$B_1(\omega_0)_b = B_2(\omega_0)_b = \cdots = B_N(\omega_0)_b = 0 \tag{4b}$$

Then, the input impedance Z_{a1}, Z_{a2}, …, Z_{aN} and Z_{b1}, Z_{b2}, ..., Z_{bN} in Fig. 4 can be calculated by

$$Z_{a1} = \frac{1}{J_{12a}^2 Z_{a2}}, \; Z_{a2} = \frac{1}{J_{23a}^2 Z_{a3}}, \; \cdots, \; Z_{aN} = \frac{1}{J_{N,N+1a}^2 Z_A} \tag{5a}$$

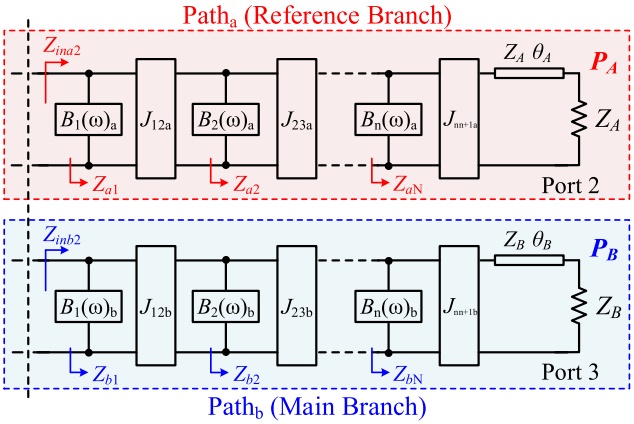

FIGURE 4. Sub-networks of the main and reference branches of the proposed FPD.

$$Z_{b1} = \frac{1}{J_{12b}^2 Z_{b2}}, \; Z_{b2} = \frac{1}{J_{23b}^2 Z_{b3}}, \; \cdots, \; Z_{bN} = \frac{1}{J_{N,N+1b}^2 Z_B} \tag{5b}$$

where

$$J_{i,i+1a} = FBW_a\sqrt{\frac{b_{ia}b_{i+1a}}{g_i g_{i+1}}}, \quad J_{N,N+1a} = \sqrt{\frac{FBW_a b_{Na}}{g_N g_{N+1} Z_A}} \tag{6a}$$

$$J_{i,i+1b} = FBW_b\sqrt{\frac{b_{ib}b_{i+1b}}{g_i g_{i+1}}}, \quad J_{N,N+1b} = \sqrt{\frac{FBW_a b_{Nb}}{g_N g_{N+1} Z_B}} \tag{6b}$$

In (6), $g_0, g_1, \ldots g_N$ are element values of low-pass prototype filter, $b_{1(a/b)}$, $b_{2(a/b)}$, …, $b_{N(a/b)}$ are the susceptance slopes, $FBW_{(a/b)}$ is the fractional bandwidth for each branch, Z_A and Z_B are the terminated impedances of outputs, respectively.

Herein, the arbitrary filter order N is considered. When N is even integer, Z_{a1} and Z_{b1} are obtained as

$$Z_{a1} = \frac{g_1}{g_{N+1}b_{1a}FBW_a}, \quad Z_{b1} = \frac{g_1}{g_{N+1}b_{1b}FBW_b} \tag{7}$$

When N is odd integer, Z_{a1} and Z_{b1} are obtained as

$$Z_{a1} = \frac{g_1 g_{N+1a}}{b_{1a}FBW}, \quad Z_{b1} = \frac{g_1 g_{N+1}}{b_{1b}FBW_b} \tag{8}$$

From (7) and (8), we can figure out the input impedances Z_{ina2} ($Z_{ina2} = Z_{a1}$) and Z_{inb2} ($Z_{inb2} = Z_{b1}$) are only related to the specified FBW, bandpass ripple L_{Ar}, and first susceptance slope b_1. Thus, the relationship between two first substance slopes for the two branches can be deduced that

$$b_{1a} = \frac{FBW_b}{FBW_a}k^2 b_{1b} \tag{9}$$

For the case of λ/2 resonator as shown in Fig. 3(b), the first-stage resonator impedance Z_{r1a} and Z_{r1b} should satisfy:

$$Z_{r1b} = \frac{FBW_b}{FBW_a}k^2 Z_{r1a} \tag{10}$$

For the case of λ/4 resonator as shown in Fig. 3(c), these two different topologies between reference planes R_1 and R_2

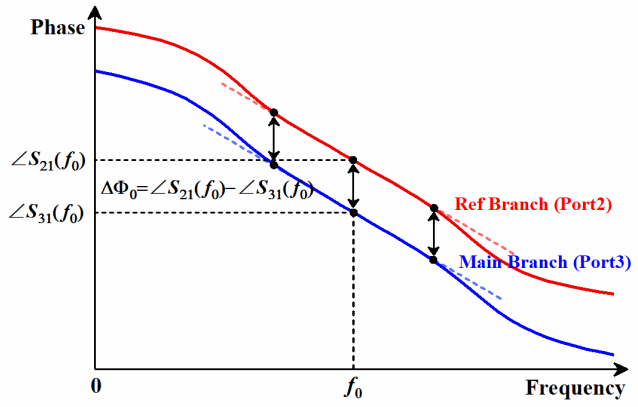

FIGURE 5. Phase properties of the proposed FPD with constant phase difference $\Delta\Phi$ ($\Delta\Phi = \angle S21 - \angle S31$).

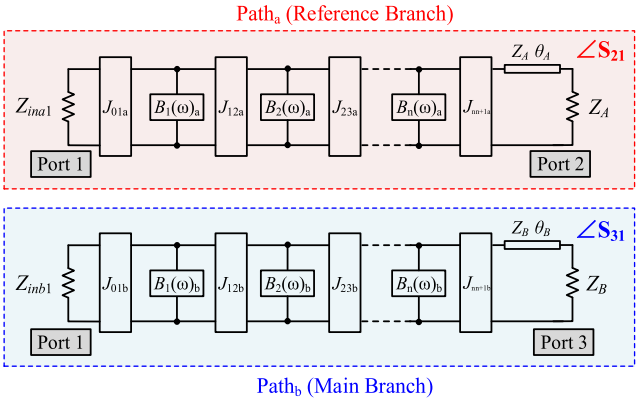

FIGURE 6. Equivalent circuit topologies of main and reference branches for the proposed FPD under the perfect isolation condition.

can be transformed by (11) in [30]. Then we can deduce the Z_{r1a} and Z_{r1b} still meet the requirement in (10).

$$\frac{K_{i,i+1}}{\sqrt{Z_{ri}Z_{r(i+1)}}} = \frac{J_{i,i+1}}{\sqrt{Y_{ri}Y_{r(i+1)}}} \tag{11}$$

Based on the above analysis, arbitrary power-division ratio k^2 and filtering responses with prescribed filter order N, bandpass ripple L_{Ar}, and fractional bandwidth FBW can be obtained for the proposed FPD. Furthermore, the higher-stage resonators can be arbitrarily designed, such as the susceptance slopes $b_{i(a/b)}$ and resonator impedances $Z_{ri(a/b)}$ ($i > 1$). The terminated impedances Z_A and Z_B can be set as arbitrary real values to realize impedance transformation.

C. ARBITRARY CONSTANT PHASE DIFFERENCE

Now, let's move to study phase properties of the proposed FPD to realize a constant phase difference $\Delta\Phi = \angle S_{21} - \angle S_{31}$ at two output ports as shown in Fig. 5.

Under the perfect isolation ($S_{32} = 0$) condition, the main and reference branches of proposed FPD can be considered as two individual paths as depicted in Fig. 6. Herein, the impedance of port 1 is changed from Z_S to Z_{ina1} and Z_{inb1}, respectively. The ABCD matrix of the two branches in Fig.6 can be calculated by

$$\begin{bmatrix} A_a & B_a \\ C_a & D_a \end{bmatrix} = [J_{1a}][B_{1a}]\cdots[J_{Na}][B_{Na}][J_{N+1a}][TL_a] \tag{12a}$$

$$\begin{bmatrix} A_b & B_b \\ C_b & D_b \end{bmatrix} = [J_{1b}][B_{1b}]\cdots[J_{Nb}][B_{Nb}][J_{N+1b}][TL_b] \tag{12b}$$

In (12), the admittance inverters $[J_{1(a/b)}], \ldots, [J_{N+1(a/b)}]$ are given in (6), susceptances $[B_{1(a/b)}], \ldots, [B_{N(a/b)}]$ consider both the $\lambda/2$ and $\lambda/4$ resonator cases as shown in Fig. 3, and $[TL_{(a/b)}]$ is the matrix of feeding line for two output ports.

For the reference branch (Path$_a$), transmission coefficient S_{21} can be derived by the ABCD matrix in (12a), that is

$$S_{21} = \frac{2\sqrt{Z_{ina1}Z_A}}{A_aZ_A + B_a + C_aZ_{ina1}Z_A + D_aZ_{ina1}} \tag{13}$$

and the output phase $\angle S_{21}$ is accordingly deduced as

$$\angle S_{21} = -\tan^{-1}\frac{B_a + C_aZ_{ina1}Z_A}{j(A_aZ_A + D_aZ_{ina1})} \tag{14}$$

For the main branch (Path$_b$), transmission coefficient S_{31} can be derived by the ABCD matrix in (12b), that is

$$S_{31} = \frac{2\sqrt{Z_{inb1}Z_B}}{A_bZ_B + B_b + C_bZ_{inb1}Z_B + D_bZ_{inb1}} \tag{15}$$

and the output phase $\angle S_{31}$ is thus obtained as

$$\angle S_{31} = -\tan^{-1}\frac{B_b + C_bZ_{inb1}Z_B}{j(A_bZ_B + D_bZ_{inb1})} \tag{16}$$

According to (13) and (16), the phase difference $\Delta\Phi(f)$ at the center frequency f_0 can be calculated as

$$\Delta\Phi(f_0) = \angle S_{21}(f_0) - \angle S_{31}(f_0) = \theta_{B0} - \theta_{A0} \tag{17}$$

In (17), θ_{A0} and θ_{B0} are the two electrical lengths of the feeding lines of the proposed FPD at the center frequency f_0, respectively.

To achieve the constant phase difference, the phase slope of these two branches should be identical as demonstrated in Fig.5, that is

$$\left.\frac{d\angle S_{21}}{df}\right|_{f=f_0} = \left.\frac{d\angle S_{31}}{df}\right|_{f=f_0} \tag{18}$$

When N is an odd integer, the formula becomes

$$\left.\frac{d\angle S_{21}}{df}\right|_{f=f_0} = -\frac{l(2\sum_{i=1}^{m-1} g_i + g_m)}{FBW_a f_0} - \frac{\prod_{i=1}^{m-1} g_i + 2[\sum_{i=1}^{m-1}(\prod_{j=1}^{m-1} g_j/g_i)]g_m}{4l\prod_{i=1}^{m} g_i f_0} \times FBW_a\pi^2 - \frac{\theta_{A0}}{f_0}$$

$$\left.\frac{d\angle S_{31}}{df}\right|_{f=f_0} = -\frac{l(2\sum_{i=1}^{m-1} g_i + g_m)}{FBW_b f_0} - \frac{\prod_{i=1}^{m-1} g_i + 2[\sum_{i=1}^{m-1}(\prod_{j=1}^{m-1} g_j/g_i)]g_m}{4l\prod_{i=1}^{m} g_i f_0} \times FBW_b\pi^2 - \frac{\theta_{B0}}{f_0}$$

where $m=(N+1)/2$, $l=1/2$ for the $\lambda/2/\lambda/4$ resonator. (19)

When N is an even integer, the formula becomes

$$\left.\frac{d\angle S_{21}}{df}\right|_{f=f_0} = -\frac{g_{N+1}\prod_{i=1}^{N/2} g_{2i}[\sum_{k=1(i\neq k)}^{N/2}(\prod_{i=1}^{N/2} g_{2i-1})/g_{2k-1}])]FBW_a\pi^2}{2l(1+g_{N+1})\prod_{i=1}^{N} g_i} - \frac{\prod_{i=1}^{N/2} g_{2i-1}[\sum_{k=1(i\neq k)}^{N/2}(\prod_{i=1}^{N/2} g_{2i})/g_{2k}]FBW_a\pi^2}{2l(1+g_{N+1})\prod_{i=1}^{N} g_i} - \frac{2l(\sum_{i=1}^{N/2} g_{2i-1} + g_{N+1}\sum_{i=1}^{N/2} g_{2i})}{(1+g_{N+1})FBW_a f_0} - \frac{\theta_{A0}}{f_0}$$

$$\left.\frac{d\angle S_{31}}{df}\right|_{f=f_0} = -\frac{g_{N+1}\prod_{i=1}^{N/2} g_{2i}[\sum_{k=1(i\neq k)}^{N/2}(\prod_{i=1}^{N/2} g_{2i-1})/g_{2k-1}])]FBW_b\pi^2}{2l(1+g_{N+1})\prod_{i=1}^{N} g_i} - \frac{\prod_{i=1}^{N/2} g_{2i-1}[\sum_{k=1(i\neq k)}^{N/2}(\prod_{i=1}^{N/2} g_{2i})/g_{2k}]FBW_b\pi^2}{2l(1+g_{N+1})\prod_{i=1}^{N} g_i} - \frac{2l(\sum_{i=1}^{N/2} g_{2i-1} + g_{N+1}\sum_{i=1}^{N/2} g_{2i})}{(1+g_{N+1})FBW_b f_0} - \frac{\theta_{B0}}{f_0}$$

where $l=1/2$ for the $\lambda/2/\lambda/4$ resonator. (20)

Compared with previous work [31] which only considers odd-order generalized bandpass network consisting of $\lambda/2$ resonators, both the odd-/even-order networks as well as $\lambda/2$ and $\lambda/4$ resonators are taken into account in this article.

Based on the above deduced formulas in (17)–(20), the arbitrary constant phase difference $\Delta\Phi = \angle S_{21} - \angle S_{31}$ of the proposed filtering FPD can be designed quantitatively.

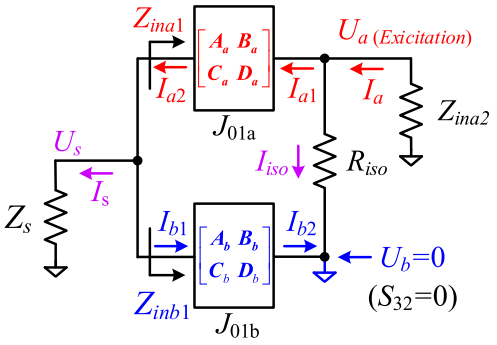

FIGURE 7. Circuit diagram of the proposed FPD with the port 2 excited.

D. ISOLATION

Isolation between two outputs is an important parameter for the PD. Ideally, when port 2 is excited, port 3 is considered as the virtual ground because no power is transmitted to it ($U_b = 0$) as shown in Fig. 7. As such, the isolation resistor R_{iso} can be determined by the voltage and current, that is

$$R_{iso} = \frac{U_a}{I_{iso}} = \frac{U_a}{-I_{b2}} \tag{21}$$

According to microwave network theory, the relationship between voltages and currents in Fig. 7 can be deduced as

$$\begin{bmatrix} U_a \\ I_a \end{bmatrix} = \begin{bmatrix} A_a & B_a \\ C_a & D_a \end{bmatrix}\begin{bmatrix} U_s \\ I_{a2} \end{bmatrix} \tag{22a}$$

$$\begin{bmatrix} U_s \\ I_{b1} \end{bmatrix} = \begin{bmatrix} A_b & B_b \\ C_b & D_b \end{bmatrix}\begin{bmatrix} 0 \\ I_{b2} \end{bmatrix} \tag{22b}$$

where the ABCD matrices of two networks with admittance inverters J_{01a} and J_{01b} are

$$\begin{bmatrix} A_a & B_a \\ C_a & D_a \end{bmatrix} = \begin{bmatrix} 0 & -j\frac{1}{J_{01a}} \\ -jJ_{01a} & 0 \end{bmatrix} \quad J_{01a} = \sqrt{\frac{FBW_a b_{r1a}}{Z_{ina1} g_0 g_1}} \tag{23a}$$

$$\begin{bmatrix} A_b & B_b \\ C_b & D_b \end{bmatrix} = \begin{bmatrix} 0 & -j\frac{1}{J_{01b}} \\ -jJ_{01b} & 0 \end{bmatrix} \quad J_{01b} = \sqrt{\frac{FBW_b b_{r1b}}{Z_{inb1} g_0 g_1}} \tag{23b}$$

then we can derive

$$U_a = A_a U_s + B_a I_{a2} \qquad I_{b2} = U_s / B_b \tag{24}$$

According to the Kirchhoff's law in circuit theory, I_{a2} in (24) can be expressed as

$$I_{a2} = I_s + I_{b1} = \frac{U_s}{R_s} + D_b I_{b2} = (\frac{1}{R_s} + \frac{D_b}{B_b})U_s \tag{25}$$

Substituting (23)–(25) into (21), the closed-form formula for isolation resistor R_{iso} of proposed FPD can be derived as

$$R_{iso} = \frac{U_a}{-I_{b2}} = \frac{g_0 g_1 \sqrt{Z_{ina1} Z_{inb1}}}{\sqrt{FBW_a FBW_b}\sqrt{b_{r1a} b_{r1b}} R_s} \tag{26}$$

Herein, the relationship between Z_{ina1} and Z_{inb1} as well as b_{r1a} and b_{r1b} in (26) should satisfy (2) and (9), respectively. Thus, the formula of R_{iso} can be rewritten as

$$R_{iso} = \frac{g_0 g_1 (1+k^2)}{b_{1a} FBW_a} \tag{27}$$

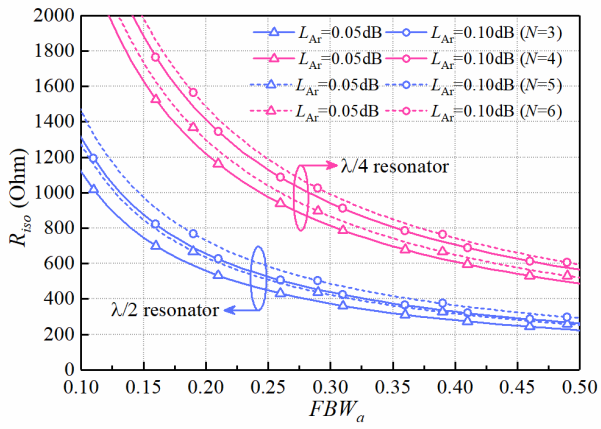

FIGURE 8. R_{iso} **versus the bandwidth** FBW_a**, filter order** N**, bandpass ripple** L_{Ar}**, and resonator type under** $k^2 = 1$ **and** $Z_{r1a} = 100\Omega$.

Fig. 8 depicts a set of design curves for $R_{\rm iso}$ as calculated from (27). We can find that $R_{\rm iso}$ of proposed FPD is related to operation bandwidth $FBW_{\rm a}$, filter order N, in-band ripple $L_{\rm Ar}$, power-division ratio k^2, resonator impedance Z_{r1a}, and resonator type (λ/2 or λ/4 resonator), but not correlated to terminated impedances of input and output. This conclusion is different to other reported formulas for $R_{\rm iso}$, such as $R_{\rm iso} = Z_L(k+1/k)$ in [32], and $R_{\rm iso} = R_S(1+k^2)^2/k^2$ in [33].

For the theoretical verification, Fig. 9 plots the simulated frequency responses of proposed FPDs with prescribed $L_{\rm Ar} = 0.1$dB, $N = 3$, $FBW_{\rm a} = 15\%$, $\Delta\Phi = 45°$, 90°, and 135°, as well as $k^2 = 1$ and 2, respectively. The impedances of three ports are set to be different, that is, $R_{\rm S} = 50\ \Omega$, $R_{\rm A} = 100\ \Omega$, and $R_{\rm B} = 200\ \Omega$. Theoretical results of circuit models show that the proposed FPDs can achieve perfect isolation ($S_{32} = 0$) over the entire frequency band under the arbitrary phase difference, terminated impedance, and power-division ratio. The good matching is indeed satisfied for S_{11}, S_{22}, and S_{33} at the same time. The designed FPDs can exactly achieve the specified 3rd-order Chebyshev filtering response and power- division ratio as illustrated in Fig. 9(a) and (b). Meanwhile, the constant phase difference 45°, 90°, and 135° are exactly realized as shown in Fig. 9(c). We can also find that the ratio k^2 has no effect on the phase responses. Till now, the proposed design concept and synthesis formulas have been well validated in theory.

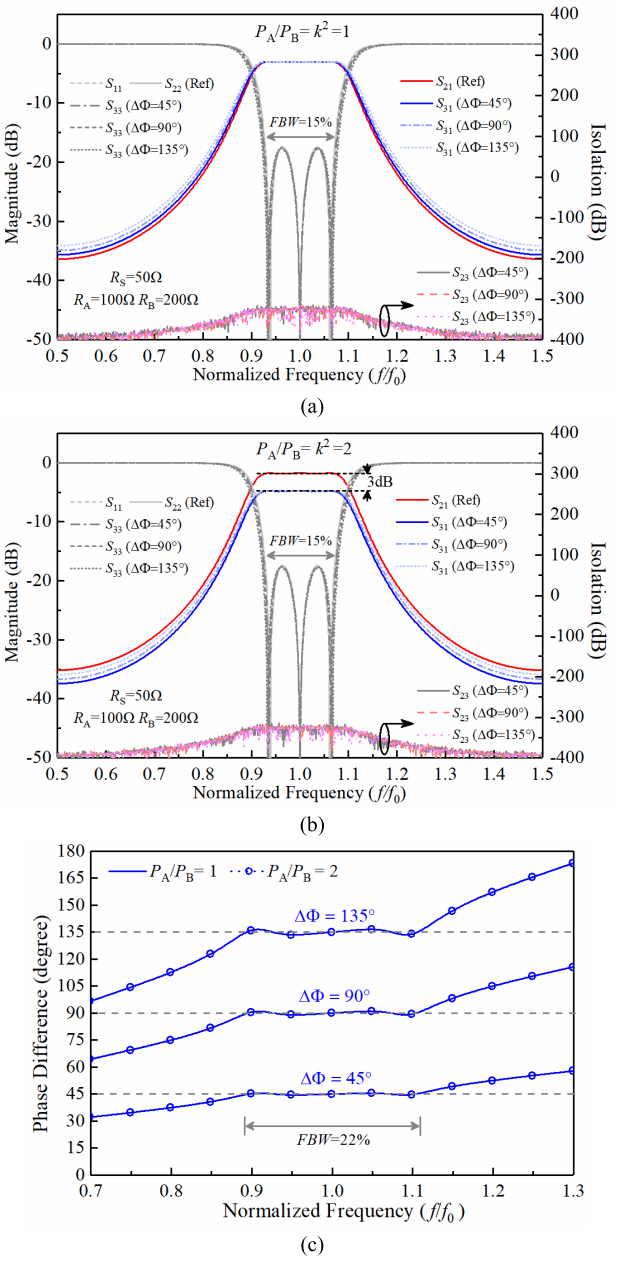

FIGURE 9. **Simulated frequency responses of proposed FPDs with prescribed** $L_{\rm Ar} = 0.1$dB, $N = 3$, $FBW_{\rm a} = 15\%$, $\Delta\Phi = 45°$, 90°, **and 135°. (a) Magnitude response with** $k^2 = 1$. **(b) Magnitude response with** $k^2 = 2$. **(c) Phase difference response with** $k^2 = 1$ **and 2.**

III. SYNTHESIS OF THIRD-ORDER 90° FILTERING POWER DIVIDER (FPD) ON λ/2 RESONATORS

In this section, synthesis procedures of the proposed third-order 90° FPD on λ/2 resonators as shown in Fig. 10 will be demonstrated. This example is implemented on microstrip-line and the used substrate is Roger's RO4003C with $\varepsilon_r = 3.55$, $\tan\delta = 0.0027$, and thickness = 0.813 mm. The FPD is centered at $f_0 = 3.0$GHz with the fractional bandwidth of 15% and the bandpass ripple of 0.1 dB. The elements of 3rd-order Chebyshev low-pass filter are $g_0 = 1$, $g_1 = 1.0316$, $g_2 = 1.1474$, $g_3 = 1.0316$, $g_4 = 1$. Three port impedances are set as $Z_{\rm S} = Z_{\rm A} = Z_{\rm B} = 50\Omega$ and power

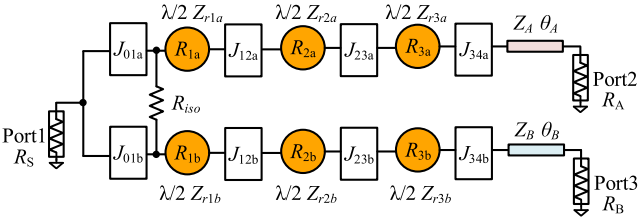

FIGURE 10. **Topology of the third-order 90° FPD on λ/2 resonators.**

division-ratio $k^2 = 1$. The detailed synthesis procedures will be given as below.

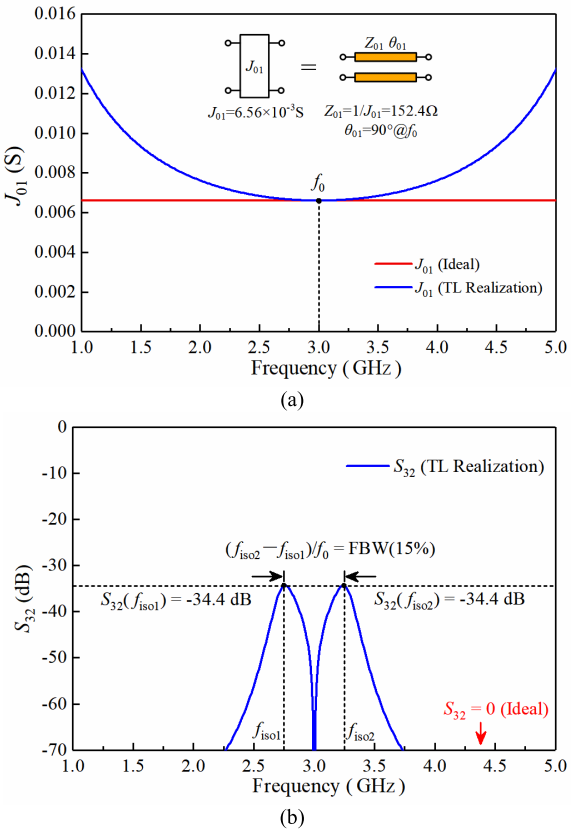

FIGURE 11. Realization of admittance inverter J_{01}. (a) Value of J_{01}. (b) S_{32}.

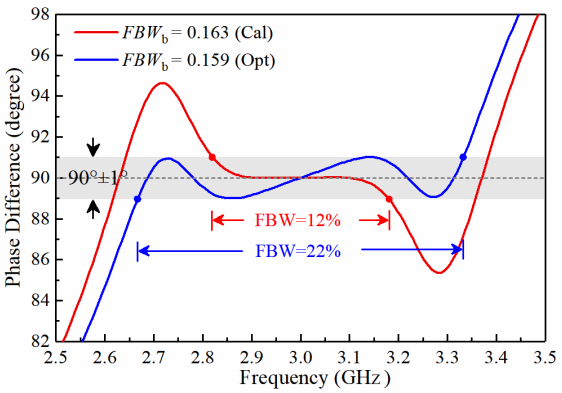

FIGURE 12. Theoretical phase response of designed third-order 90° FPD.

A. SYNTHESIS PROCEDURES

1). Achieve the 90° phase difference at two output ports. The electrical length difference of θ_{A0} and θ_{B0} for the two feeding lines can be determined at first according to $\Delta\Phi_0 = 90°$ at f_0 as

$$\Delta\Phi_0 = \theta_B(f_0) - \theta_A(f_0) = \theta_{B0} - \theta_{A0} = 90° \tag{28}$$

To achieve constant 90° phase difference, this FPD must be satisfied with the relation concerning the phase slope in (18). Meanwhile, the close-form formula of phase slope for the third-order 90° FPD can be derived from (19), that is

$$\left.\frac{d\angle S_{21}}{df}\right|_{f=f_0} = \left(-\frac{2g_1+g_2}{FBW_a\pi} - \frac{g_1+2g_2}{4g_1g_2}FBW_a\pi\right)\frac{\pi}{f_0} - \frac{\theta_{A0}}{f_0}$$
$$= \left.\frac{d\angle S_{31}}{df}\right|_{f=f_0} = \left(-\frac{2g_1+g_2}{FBW_b\pi} - \frac{g_1+2g_2}{4g_1g_2}FBW_b\pi\right)\frac{\pi}{f_0} - \frac{\theta_{B0}}{f_0} \tag{29}$$

In this design, the bandwidth of reference branch is set equal to the prescribed bandwidth of 15%, that is, $FBW_a = 0.15$. Then, the theoretical value of FBW_b can be calculated as 0.163 from (29). To further extend phase shift bandwidth by introducing small phase ripple, the FBW_b can be chosen slightly smaller than calculated one as shown in Fig. 12.

2) Determine resonator impedances and isolation resistor. For the practical implementation, isolation resistor R_{ios} can only be set to several standard values. In this case, we choose $R_{ios} = 464\ \Omega$ in E96 series. For the λ/2 resonator, the resonator impedance Z_{r1a} can be derived from (27), that is

$$Z_{r1a} = \frac{\pi FBW_a R_{iso}}{2g_0g_1(1+k^2)} = 53\ \Omega \tag{30}$$

Based on (10), resonator impedance Z_{r1b} is obtained as

$$Z_{r1b} = \frac{FBW_b}{FBW_a}k^2 Z_{r1a} = 56.1\ \Omega \tag{31}$$

According to the theoretical analysis in (7) and (8), the higher-stage resonators can be arbitrarily designed. Herein, we readily set $Z_{r2a} = Z_{r2b} = Z_{r3a} = Z_{r3b} = 70\ \Omega$.

3). Calculate the values of all admittance inverters. Since the resonator impedances $Z_{r1a/b} \sim Z_{r3a/b}$, fractional bandwidth $FBW_{a/b}$, and element values $g_0 \sim g_4$ are obtained, the values of admittance inverters can be determined as

$$J_{01a} = \sqrt{\frac{FBW_a b_{r1a}}{Z_{ina1}g_0g_1}};\quad J_{01b} = \sqrt{\frac{FBW_b b_{r1b}}{Z_{inb1}g_0g_1}} \tag{32a}$$

$$J_{12a} = FBW_a\sqrt{\frac{b_{r1a}b_{r2a}}{g_1g_2}};\quad J_{12b} = FBW_b\sqrt{\frac{b_{r1b}b_{r2b}}{g_1g_2}} \tag{32b}$$

$$J_{23a} = FBW_a\sqrt{\frac{b_{r2a}b_{r3a}}{g_2g_3}};\quad J_{23b} = FBW_b\sqrt{\frac{b_{r2b}b_{r3b}}{g_2g_3}} \tag{32c}$$

$$J_{34a} = \sqrt{\frac{FBW_a b_{r3a}}{R_A g_3 g_4}};\quad J_{34b} = \sqrt{\frac{FBW_b b_{r3a}}{R_B g_3 g_4}} \tag{32d}$$

In (32), $J_{01a} = 6.56$mS, $J_{12a} = 3.56$mS, $J_{23a} = 3.09$mS, $J_{34a} = 8.08$mS; $J_{01b} = 6.56$mS, $J_{12b} = 3.71$mS, $J_{23b} = 3.36$mS, $J_{34b} = 8.42$ mS.

4). Map above-calculated circuit parameters into physical dimensions. At first, J_{01} admittance inverter can be realized by a λ/4 transmission line with characteristic impedance $Z_{01} = 1/J_{01}$. Herein, $Z_{01a} = Z_{01b} = 152.4\ \Omega$ is set to achieve $J_{01a} = J_{01b} = 6.56$ mS. The extracted curve of J_{01} value is shown in Fig. 11(a). Compared with the theoretical results in Fig. 9, the perfect isolation ($S_{32} = 0$) can only be obtained at f_0. It is because the J_{01} is deviated from the desired value as shown in Fig. 11(a), resulting in

the S_{32} gradually increasing with respect to the frequency. We find the worst S_{32} is occurred at the edge of operation band, that is, $f_{iso1} = f_0(1–FBW/2)$ and $f_{iso2} = f_0(1+FBW/2)$. Then, the S_{32} decreases rapidly due to the transmitted energy is suppressed by filtering response.

Secondly, two types of λ/2 resonators are utilized to construct the proposed filtering 90° PD, that is, open-ended and short-end λ/2 resonators. On the one hand, it validates the proposed design method is independent of the resonator realization. On the other hand, the combination of open-ended and short-end resonators can effectively suppress the harmonics as studied in [34]. The strip width and length of microstrip-line resonators is determined by using LineCalc Tools in ADS based on the known circuit parameters.

Thirdly, coupling coefficients and external quality factor are determined from the values of admittance inverters as

$$M_{i,i+1} = \frac{J_{i,i+1}}{\sqrt{b_i b_{i+1}}}; \qquad Q_{eo} = \frac{b_N}{\sqrt{R_L J_{N,N+1}^2}} \tag{33}$$

Based on (32) and (33), we can derive that $M_{12a} = 0.138$, $M_{23a} = 0.138$, $Q_{eoa} = 6.877$, $M_{12b} = 0.146$, $M_{23b} = 0.146$, $Q_{eob} = 6.496$. Using the method proposed in [35], the physical dimensions of M_{12}, M_{23}, and Q_{eo} can be extracted and the relevant results are provided in Fig. 13. Now, the overall dimensions can be determined. To compensate for certain unexpected effects in quasi-TEM microstrip line structure, slight adjustments are further executed in the simulation.

B. EXPERIMENTAL RESULT

Based on the above-described procedures, the prototype of third-order 90° FPD is designed, fabricated, and measured. Fabricated photograph and physical layout with dimensions are displayed in Fig. 14. The simulation and measurement are executed by the full-wave simulator NI AWR software 14.0 and the network analyzer R&S ZNB20, respectively.

Fig. 15(a) shows the magnitude response of the proposed PD. We can find the desired power division and bandpass responses are indeed satisfactorily realized with the central frequency at 3 GHz, and the fractional bandwidth of 16%. Within the passband, the power is equally split with the $|S_{21}|$ and $|S_{31}|$ of 3+1.63 dB and 3+1.78 dB. The measured in-band insertion loss, including the loss of SMA connectors, is less than 1.78 dB at two outputs. Besides, the maximum amplitude imbalance of the proposed 90° PD is only 0.15 dB. Meanwhile, simulated and measured results of S_{11}, S_{22}, and S_{33} are presented to exhibit that the return loss is better than 12 dB with bandwidth of 16% for all three I/O ports. What's more, the measured isolation is better than 25 dB over the whole passband. The slight discrepancies between simulated and measured results may be due to unexpected approximation in simulation and tolerance in fabrication.

Fig. 15(b) shows the phase response of the proposed PD. We can observe that the constant 90° phase difference with small phase deviation is obtained as required. The measured phase deviation is less than ±2.5° from 2.63 to 3.43 GHz

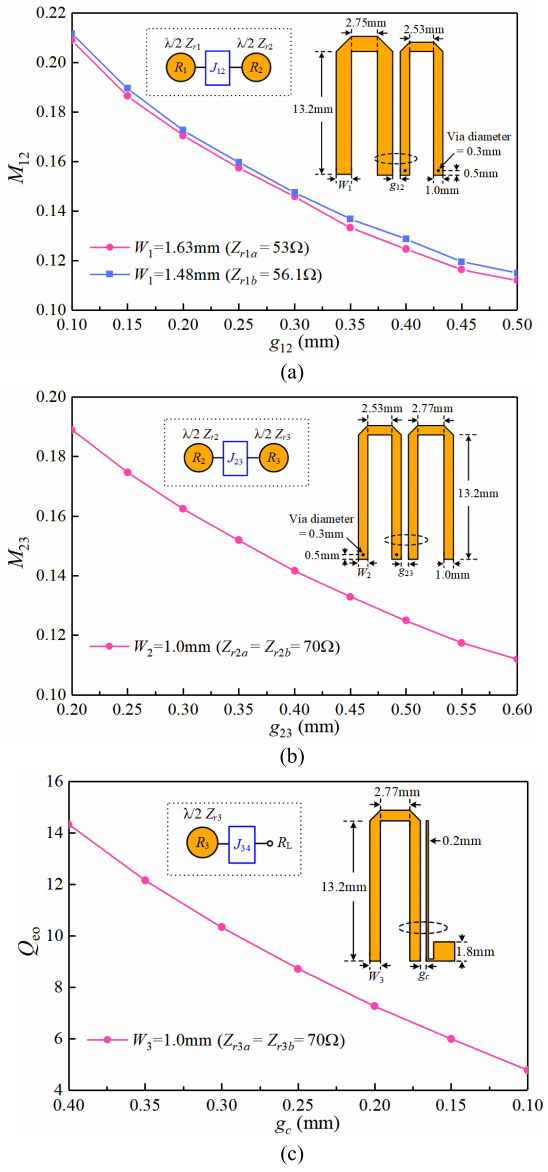

FIGURE 13. (a) Extracted M_{12} versus coupling gap g_{12}. (b) Extracted M_{23} versus coupling gap g_{23}. (c) Extract Q_{eo} versus coupling gap g_c.

(26.4% in fraction). The simulated and measured results are found in general agreement with each other. Meanwhile, the prescribed power division, filtering response, constant phase difference, and good isolation are all satisfactorily achieved. Furthermore, the proposed 90° PD only occupies the overall size of 45.5 mm × 58 mm or 0.46 λ_0× 0.58 λ_0 (λ_0 is the wavelength in free space at 3.0 GHz).

IV. SYNTHESIS OF SIXTH-ORDER 120° FILTERING POWER DIVIDER (FPD) ON λ/4 RESONATORS

To verify the design flexibility, a sixth-order 120° FPD on λ/4 resonators as shown in Fig. 16 will be synthesized and designed in this section. The FPD is implemented on the same substrate used above and is centered at 3.0 GHz with the fractional bandwidth of 25%. The elements of sixth-order Chebyshev low-pass filter are $g_0 = 1$, $g_1 = 0.8206$,

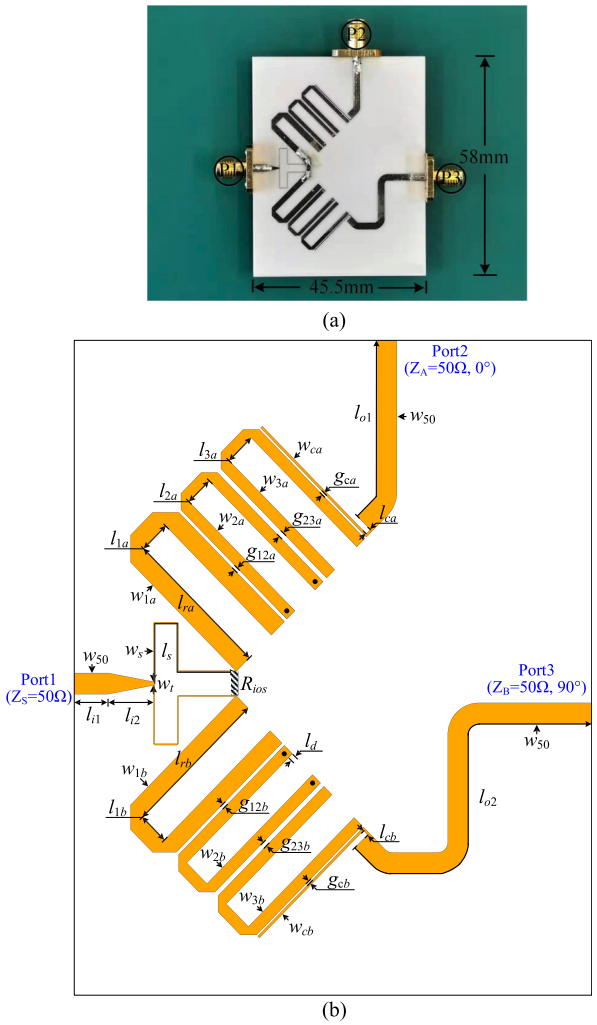

FIGURE 14. (a) Photograph of the fabricated proposed third-order 90° FPD. (b) Layout with dimensions (in mm): $l_{ra} = l_{rb} = 13.2$, $l_{1a} = l_{1b} = 2.75$, $l_{2a} = l_{2b} = 2.53$, $l_{3a} = l_{3b} = 2.77$, $w_{1a} = 1.63$, $w_{1b} = 1.48$, $w_{2a} = w_{3a} = w_{2b} = w_{3b} = 1$, $w_{ca} = w_{cb} = 0.2$, $g_{12a} = 0.31$, $g_{23a} = 0.44$, $g_{ca} = 0.19$, $g_{12b} = 0.29$, $g_{23b} = 0.42$, $g_{cb} = 0.17$, $l_{ca} = l_{cb} = 0.5$, $D = 0.3$, $l_d = 0.5$, $l_s = 16.2$, $w_s = 0.1$, $w_{50} = 1.8$, $w_t = 0.3$, $l_{i1} = 3$, $l_{i2} = 4$, $l_{o1} = 17.8$, $l_{o2} = 33.6$.

$g_2 = 1.3769$, $g_3 = 1.7285$, $g_4 = 1.5445$, $g_5 = 1.5409$, $g_6 = 0.7332$, $g_7 = 1.1192$ for the 25 dB in-band return loss. The port impedances are set as $Z_S = 50\ \Omega$ for port 1 and $Z_A = Z_B = 100\Omega$ for port 2 and 3, respectively. For comparison, the power division-ratio is also set as $k^2 = 1$.

A. SYNTHESIS PROCEDURES

1). Achieve the 120° phase difference at two output ports. The electrical length difference of θ_{A0} and θ_{B0} for the two feeding lines can be determined at first as

$$\Delta\Phi_0 = \theta_B(f_0) - \theta_A(f_0) = \theta_{B0} - \theta_{A0} = 120^\circ \tag{34}$$

To achieve constant 120° phase difference, the proposed FPD should satisfy synthesis equation in (18). Meanwhile, close-form formula of phase slope for the designed

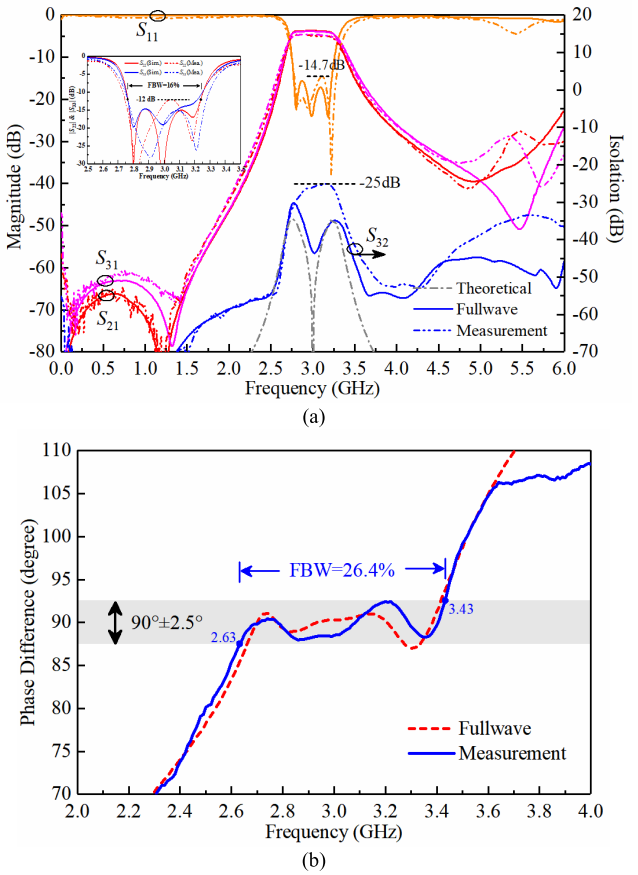

FIGURE 15. Simulated and measured frequency responses of proposed third-order filtering 90° FPD. (a) Magnitude response. (b) Phase response.

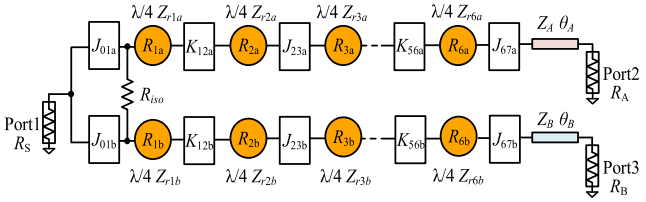

FIGURE 16. Topology of the sixth-order 120° FPD on λ/4 resonators.

sixth-order 120° PD can be derived from (20), that is

$$\left.\frac{d\angle S_{21}}{df}\right|_{f=f_0} = \left(-\frac{4E}{IFBW_a\pi} - \frac{F+G}{4HI}FBW_a\pi\right)\frac{\pi}{f_0} - \frac{\theta_{A0}}{f_0}$$
$$= \left.\frac{d\angle S_{31}}{df}\right|_{f=f_0} = \left(-\frac{4E}{IFBW_b\pi} - \frac{F+G}{4HI}FBW_b\pi\right)\frac{\pi}{f_0} - \frac{\theta_{B0}}{f_0} \tag{35}$$

where

$$E = g_1 + g_3 + g_5 + (g_2 + g_4 + g_6)g_7 \tag{36a}$$
$$F = g_1g_3g_5[g_4g_6 + g_2(g_4 + g_6)] \tag{36b}$$
$$G = g_2g_4g_6g_7[g_3g_5 + g_1(g_3 + g_5)] \tag{36c}$$
$$H = g_1g_2g_3g_4g_5g_6 \tag{36d}$$
$$I = 1 + g_7 \tag{36e}$$

In this design, $FBW_a = 0.25$. Then, the theoretical value of FBW_b is calculated as 0.268 from (35).

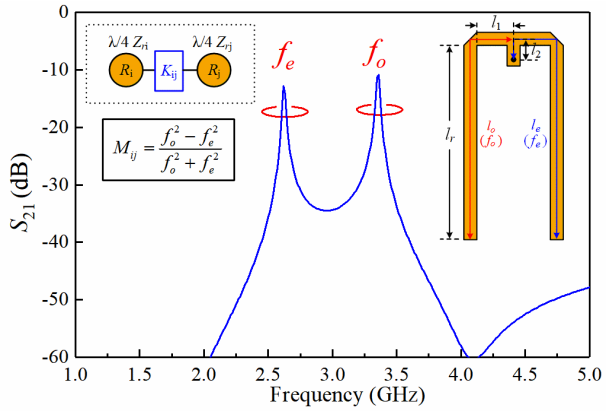

FIGURE 17. Extract method for the physical dimensions of *K*-inverter.

2) Determine resonator impedances and isolation resistor. To show the design flexibility, we choose $R_{\rm iso} = 453\Omega$ in E96 series in this case, which is different from the previous design. For the λ/4 resonator, $b_{\rm r1a} = \pi/(4Z_{\rm r1a})$. The resonator impedance $Z_{\rm r1a}$ can be determined from (27), that is

$$Z_{r1a} = \frac{\pi FBW_a R_{iso}}{4g_0 g_1 (1+k^2)} = 54.2\,\Omega \tag{37}$$

Based on (10), resonator impedance $Z_{\rm r1b}$ is obtained as

$$Z_{r1b} = \frac{FBW_b}{FBW_a} k^2 Z_{r1a} = 56.4\ \Omega \tag{38}$$

As discussed previously, higher-stage resonators can be arbitrarily designed for the proposed PD. Herein, we readily set $Z_{\rm r2a} = 54.2\Omega$, $Z_{\rm r2b} = 56.4\Omega$, $Z_{\rm r3a} = Z_{\rm r3b} = \ldots = 77\Omega$.

3). Calculate the values of admittance inverters. In this design, the value of *J*-inverter can be derived from (32a)–(32d), while the value of *K*-inverter can be obtained as

$$K_{12a} = FBW_a\sqrt{\frac{x_{r1a}x_{r2a}}{g_1 g_2}};\quad K_{12b} = FBW_b\sqrt{\frac{x_{r1b}x_{r2b}}{g_1 g_2}} \tag{39a}$$

$$K_{34a} = FBW_a\sqrt{\frac{x_{r3a}x_{r4a}}{g_3 g_4}};\quad K_{34b} = FBW_b\sqrt{\frac{x_{r3b}x_{r4b}}{g_3 g_4}} \tag{39b}$$

$$K_{56a} = FBW_a\sqrt{\frac{x_{r5a}x_{r6a}}{g_5 g_6}};\quad K_{56b} = FBW_b\sqrt{\frac{x_{r5b}x_{r6b}}{g_5 g_6}} \tag{39c}$$

In (39), $x_{\rm ria/b} = Z_{\rm ria/b}\pi/4$ for the λ/4 resonator. Based on (32) and (39), we can derive that $J_{01a} = 6.64$mS, $K_{12a} = 10.01\Omega$, $J_{23a} = 1.97$mS, $K_{34a} = 9.25\Omega$, $J_{45a} = 1.65$mS, $K_{56a} = 14.22\Omega$, $J_{67a} = 5.57$mS; $J_{01b} = 6.64$mS, $K_{12b} = 10.83\Omega$, $J_{23a} = 2.01$mS, $K_{34a} = 9.62\Omega$, $J_{45a} = 1.72$mS, $K_{56a} = 14.79\Omega$, $J_{67a} = 5.68$mS.

4). Map the calculated circuit parameters into physical dimensions. The J_{01} admittance inverter is also realized by a λ/4 transmission line with impedance $Z_{01} = 1/J_{01}$. Herein, $Z_{01a} = Z_{01b} = 150.6\ \Omega$ is set to achieve $J_{01a} = J_{01b} = 6.64$ mS. The strip width and length of the microstrip line can be mapped by using LineCalc Tools in ADS as well.

Secondly, the *K*-inverter is realized by the short-ended stub as depicted in Fig. 17. Physical dimensions

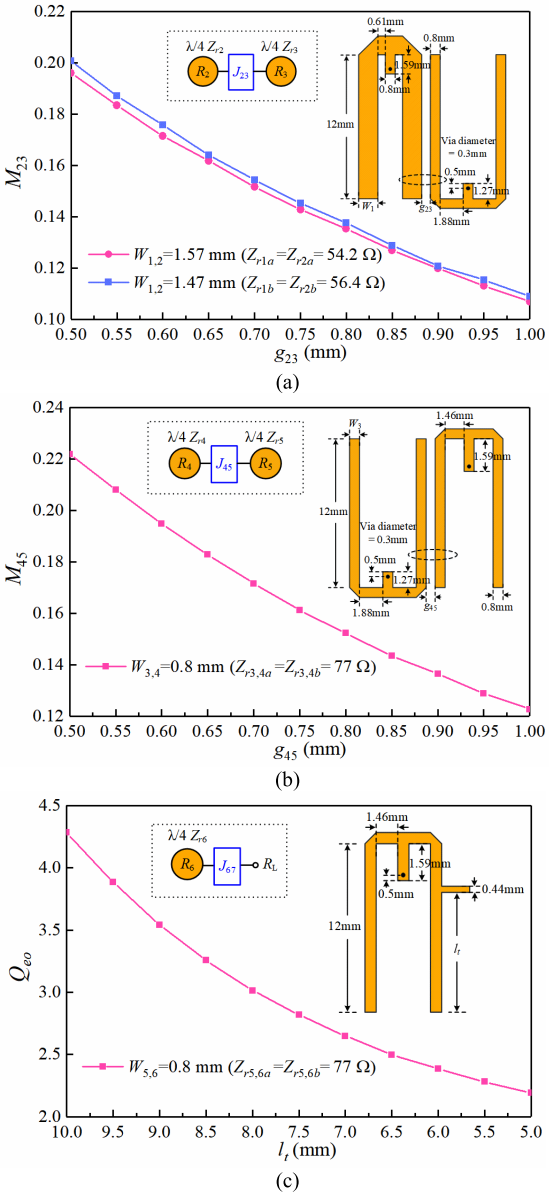

FIGURE 18. (a) Extracted M_{23} versus coupling gap g_{23}. (b) Extracted M_{45} versus coupling gap g_{45}. (c) Extract $Q_{\rm eo}$ versus tap position l_t.

(l_1, l_2, and $l_{\rm r}$) can be directly extracted according to the given coupling coefficient $M_{\rm ij}$ and center frequency f_0. The design formulas are thus deduced as

$$l_1 = \frac{M_{ij}\pi c}{4f_0\sqrt{\varepsilon_{re}}(M_{ij}+1-\sqrt{1-M_{ij}^2})} - l_r \tag{40a}$$

$$l_2 = \frac{M_{ij}\pi c}{4f_0\sqrt{\varepsilon_{re}}(M_{ij}-1+\sqrt{1-M_{ij}^2})} - l_r - l_1 \tag{40b}$$

where c is the light velocity and $\varepsilon_{\rm re}$ is effective dielectric constant.

Thirdly, coupling coefficients and external quality factor can be determined by (33). Therefore, we can derive that $M_{12a} = 0.235$, $M_{23a} = 0.162$, $M_{34a} = 0.153$, $M_{45a} = 0.162$, $M_{56a} = 0.235$, $Q_{eoa} = 3.282$; $M_{12b} = 0.245$, $M_{23a} = 0.169$,

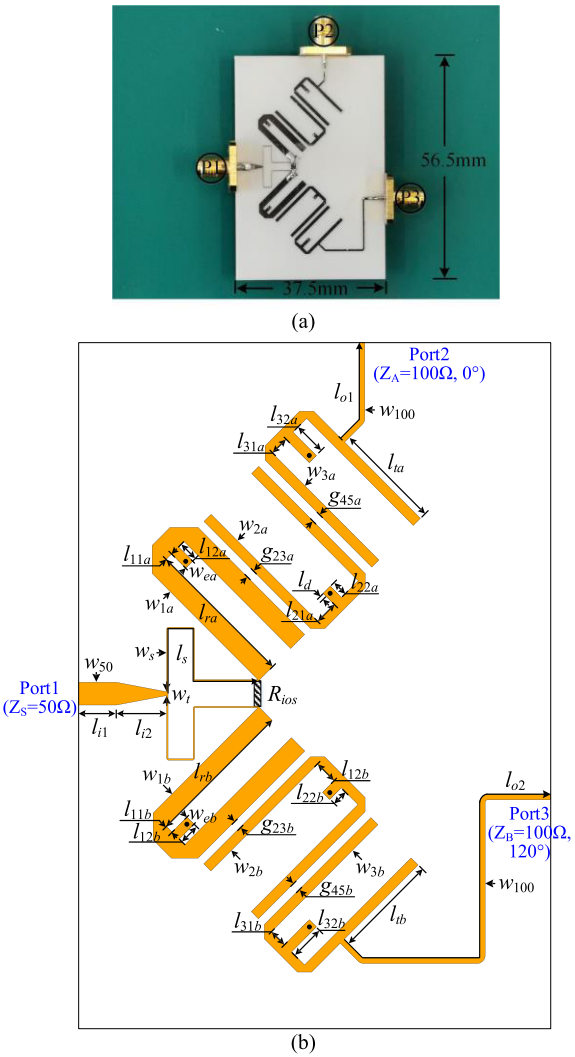

FIGURE 19. **(a) Photograph of the fabricated proposed sixth-order 120° FPD. (b) Layout with dimensions (in mm): $l_{ra} = l_{rb} = 12$, $l_{11a} = 0.61$, $l_{12a} = 1.59$, $l_{21a} = 1.88$, $l_{22a} = 1.27$, $l_{31a} = 1.54$, $l_{32a} = 2.63$, $l_{11b} = 0.63$, $l_{12b} = 1.67$, $l_{21b} = 1.88$, $l_{22b} = 1.31$, $l_{31b} = 1.46$, $l_{32b} = 2.81$, $w_{1a} = 1.57$, $w_{1b} = 1.47$, $w_{2a} = w_{3a} = w_{2b} = w_{3b} = 0.8$, $w_{ea} = 0.8$, $g_{23a} = 0.68$, $g_{45a} = 0.72$, $g_{23b} = 0.65$, $g_{45b} = 0.66$, $l_{ta} = 8.54$, $l_{tb} = 8.33$, $D = 0.3$, $l_d = 0.4$, $l_s = 16.2$, $w_s = 0.13$, $w_{50} = 1.8$, $w_{100} = 0.44$, $w_t = 0.3$, $l_{i1} = 3$, $l_{i2} = 4$, $l_{o1} = 8.35$, $l_{o2} = 29.53$.**

$M_{34a} = 0.159$, $M_{45a} = 0.169$, $M_{56a} = 0.245$, $Q_{eoa} = 3.156$. Among them, the physical dimensions of M_{12}, M_{34}, and M_{56} can be determined by (40). Meanwhile, the physical dimensions of M_{23}, M_{45}, and Q_{eo} can be extracted by using the approach in [35] and relevant results are depicted in Fig. 18. Different from the previous design, J_{67} ($J_{N,N+1}$) is realized by tapped line to show the design flexibility. As such, overall physical dimensions of proposed FPD can be determined. The final layout and fabricated photograph are shown in Fig. 19 after minor fine tuning in the fullwave simulation.

B. EXPERIMENTAL RESULT

The simulated and measured frequency responses of the designed sixth-order 120° FPD are portrayed in Fig. 20. In our measurement, well-known TRL calibration technique is applied to remove the parasitic effects of SMA connectors.

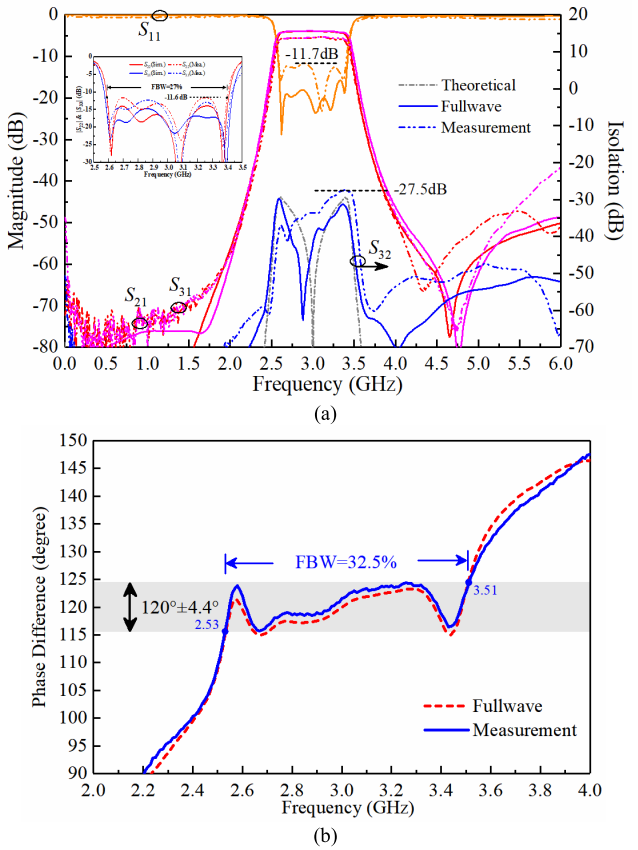

FIGURE 20. **Simulated and measured frequency responses of proposed sixth-order 120° FPD. (a) Magnitude response. (b) Phase response.**

As shown in Fig. 20(a), the functions of power division and filtering response are indeed obtained as required. Within the passband, the power is equally split with the $|S_{21}|$ and $|S_{31}|$ of 3+2.36 dB and 3+2.57 dB. Measured insertion loss is less than 2.57 dB, which is 0.79 dB higher than the previous third-order design, as probably caused by the extra losses owing to the increased stages and loaded pins [30]. However, the measured maximum amplitude imbalance of proposed 120° FPD is only 0.21 dB. The measured S_{11}, S_{22}, and S_{33} magnitudes are all better than -11.6 dB with the bandwidth of 27% for all three input and output ports. The measured return losses are worse than simulated results due to unexpected fabrication tolerance and transition losses in the measurement. But the simulated and measured filtering responses can be still found in good accordance with each other, which exhibit desired sixth-order response with sharp rejection skirt. More importantly, good isolation is obtained as expected and the measured result is better than 27.5 dB over the whole passband.

Fig. 20(b) shows the phase response of the proposed PD. The wideband constant 120° phase difference is obtained as desired. The measured phase deviation is less than ±4.4° from 2.53 to 3.51 GHz with the bandwidth of 32.5%. The experimental results well verify that proposed design theory successfully integrates power divider, filter, phase shifter, and impedance transformer into only one component.

TABLE 1. Property and measured performance comparison with other reported power dividers in state-of-art.

Ref.	f_0	FBW	Filter order	Phase difference	Return loss	Insertion loss	Isolation	Isolation region	Filtering function	Arbitrary phase shift	Isolation outputs	Impedance transform
[10]	0.9	4.2%	4	In-phase	>19	<3.0	>11	W.B	✔	✖	✔	✖
[12]	1	43%	2	In-phase	>20	0.3(f_0)	>20	0.76-1.18 (43.2%)	✔	✖	✔	✖
[14]	1.2	3.5%	2	In-Phase /Out.-phase	>16	<1.4	>30	W.B	✔	✖	✔	✖
[19]	6.0	110%	4	In-Phase /Out.-phase	>12	<2.2	>11	W.B	✔	✖	✔	✖
[25]	2.0	30%	✖	45°±3.15° 90°±1.42°	>14.5	<1.57	>20	1.7-2.3 (30%)	✖	✔	✔	✖
[28]	10	10.8%	3	90°±5.5°	>13.5	<1.90	✖	✖	✔	✔	✖	✖
Work 1	3.0	16%	3	90°±2.5°	>14.7	<1.78	>25	W.B	✔	✔	✔	✔
Work 2	3.0	27%	6	120°±4.4°	>11.7	<2.57	>27.5	W.B	✔	✔	✔	✔

The overall size is only 37.5 mm × 56.5 mm or 0.38 $\lambda_0 \times$ 0.57 λ_0 as shown in Fig. 19(a). Furthermore, comparisons in a few critical parameters to other reported PDs in state-of-art are listed in Table 1. It also has several advantages, such as low cost, simple geometry, small phase deviation and amplitude imbalance, easiness for design and fabrication.

V. CONCLUSION

In this paper, a new class of filtering power dividers with constant phase difference and good isolation is proposed for the first time. Compared with traditional counterparts, the arbitrary constant phase difference at two output ports can be realized within a prescribed bandwidth. The desired multiple functions of power dividing, bandpass filtering, phase shifting, and impedance transforming are realized in a single one component. Moreover, the proposed synthesis method can effectively determine the circuit parameters and physical dimensions for our presented power dividers with prescribed power-division ratio k^2, phase difference $\Delta\Phi$, operation bandwidth FBW, filter order N, bandpass ripple L_{Ar}, and terminated impedances Z_S, Z_A, and Z_B. To validate design concept and theory, two practical prototypes have been successfully designed, fabricated, and measured.

REFERENCES

[1] N. Yang, C. Caloz, and K. Wu, "Greater than the sum of its parts," *IEEE Microw. Mag.*, vol. 11, no. 4, pp. 69–82, Jun. 2010.

[2] R. Gómez-García, J. Rosario-De Jesus, and D. Psychogiou, "Multi-band bandpass and bandstop RF filtering couplers with dynamically-controlled bands," *IEEE Access*, vol. 6, pp. 32321–32327, 2018.

[3] H. Jin, G. Q. Luo, W. Wang, W. Che, and K.-S. Chin, "Integration design of millimeter-wave filtering patch antenna array with SIW four-way anti-phase filtering power divider," *IEEE Access*, vol. 7, pp. 49804–49812, 2019.

[4] T.-L. Wu, Y.-M. Pan, P.-F. Hu, and S.-Y. Zheng, "Design of a low profile and compact omnidirectional filtering patch antenna," *IEEE Access*, vol. 5, pp. 1082–1089, 2017.

[5] C.-F. Chen, K.-W. Zhou, R.-Y. Chen, Z.-C. Wang, and Y.-H. He, "Design of a microstrip diplexer-integrated filtering power divider," *IEEE Access*, vol. 7, pp. 106514–106520, 2019.

[6] Y. C. Li, Q. Xue, and X. Y. Zhang, "Single- and dual-band power dividers integrated with bandpass filters," *IEEE Trans. Microw. Theory Techn.*, vol. 61, no. 1, pp. 69–76, Jan. 2013.

[7] K. Song, "Compact filtering power divider with high frequency selectivity and wide stopband using embedded dual-mode resonator," *Electron. Lett.*, vol. 51, no. 6, pp. 495–497, Mar. 2015.

[8] K. Song, M. Fan, F. Zhang, Y. Zhu, and Y. Fan, "Compact triple-band power divider integrated bandpass-filtering response using short-circuited SIRs," *IEEE Trans. Compon., Packag., Manuf. Technol.*, vol. 7, no. 7, pp. 1144–1150, Jul. 2017.

[9] R. Gómez-García, R. Loeches-Sánchez, D. Psychogiou, and D. Peroulis, "Single/multi-band Wilkinson-type power dividers with embedded transversal filtering sections and application to channelized filters," *IEEE Trans. Circuits Syst. I, Reg. Papers*, vol. 62, no. 6, pp. 1518–1527, Jun. 2015.

[10] C.-F. Chen, T.-Y. Huang, T.-M. Shen, and R.-B. Wu, "Design of miniaturized filtering power dividers for system-in-a-package," *IEEE Compon., Packag., Manuf. Technol.*, vol. 3, no. 10, pp. 1663–1672, Oct. 2013.

[11] X. Y. Zhang, K.-X. Wang, and B.-J. Hu, "Compact filtering power divider with enhanced second-harmonic suppression," *IEEE Microw. Wireless Compon. Lett.*, vol. 23, no. 9, pp. 483–485, Sep. 2013.

[12] Y. Wu, Z. Zhuang, Y. Liu, L. Deng, and Z. Ghassemlooy, "Wideband filtering power divider with ultra-wideband harmonic suppression and isolation," *IEEE Access*, vol. 4, pp. 6876–6882, 2016.

[13] X. Yu and S. Sun, "A novel wideband filtering power divider with embedding three-line coupled structures," *IEEE Access*, vol. 6, pp. 41280–41290, 2018.

[14] C.-F. Chen and C.-Y. Lin, "Compact microstrip filtering power dividers with good in-band isolation performance," *IEEE Microw. Wireless Compon. Lett.*, vol. 24, no. 1, pp. 17–19, Jan. 2014.

[15] S.-F. Chao and W.-C. Lin, "Filtering power divider with good isolation performance," *Electron. Lett.*, vol. 50, no. 11, pp. 815–817, May 2014.

[16] Y. Deng, J. Wang, L. Zhu, and W. Wu, "Filtering power divider with good isolation performance and harmonic suppression," *IEEE Microw. Wireless Compon. Lett.*, vol. 26, no. 12, pp. 984–986, Dec. 2016.

[17] S. Chen, Y. Yu, and M. Tang, "Planar out-of-phase Gysel power divider with high power splitting ratio," *Electron. Lett.*, vol. 51, no. 24, pp. 2010–2012, Nov. 2015.

[18] M. Liao, Y. Wu, Y. Liu, and J. Gao, "Impedance-transforming dual-band out-of-phase power divider," *IEEE Microw. Wireless Compon. Lett.*, vol. 24, no. 8, pp. 524–526, Aug. 2014.

[19] H. Zhu, Z. Cheng, and Y. J. Guo, "Design of wideband in-phase and out-of-phase power dividers using microstrip-to-slotline transitions and slotline resonators," *IEEE Trans. Microw. Theory Techn.*, vol. 67, no. 4, pp. 1412–1424, Apr. 2019.

[20] Y.-X. Guo, K.-W. Khoo, and L. C. Ong, "Wideband circularly polarized patch antenna using broadband baluns," *IEEE Trans. Antennas Propag.*, vol. 56, no. 2, pp. 319–326, Feb. 2008.

[21] C. Lin, F.-S. Zhang, Y.-C. Jiao, F. Zhang, and X. Xue, "A three-fed microstrip antenna for wideband circular polarization," *IEEE Antennas Wireless Propag. Lett.*, vol. 9, pp. 359–362, 2010.
[22] C.-H. Tseng and C.-L. Chang, "Improvement of return loss bandwidth of balanced amplifier using metamaterial-based quadrature power splitters," *IEEE Microw. Wireless Compon. Lett.*, vol. 18, no. 4, pp. 269–271, Apr. 2008.
[23] S. Z. Ibrahim, A. Abbosh, and M. Bialkowski, "Design of wideband six-port network formed by in-phase and quadrature Wilkinson dividers," *IET Microw., Antennas Propag.*, vol. 6, no. 11, pp. 1215–1220, Aug. 2012.
[24] Y.-C. Tsai, J.-L. Kuo, J.-H. Tsai, K.-Y. Lin, and H. Wang, "A 50–70 GHz I/Q modulator with improved sideband suppression using HPF/LPF based quadrature power splitter," in *IEEE MTT-S Int. Microw. Symp. Dig.*, Jun. 2011, pp. 1–4.
[25] J. Zhou, H. J. Qian, and X. Luo, "Compact wideband phase shifter using microstrip self-coupled line and broadside-coupled microstrip/CPW for multiphase feed-network," *IEEE Microw. Wireless Compon. Lett.*, vol. 27, no. 9, pp. 791–793, Sep. 2017.
[26] H.-R. Ahn, "Compact CVT-/CCT-unequal power dividers for high-power division ratios and design methods for arbitrary phase differences," *IEEE Trans. Microw. Theory Techn.*, vol. 62, no. 12, pp. 2954–2964, Dec. 2014.
[27] Y.-P. Lyu, L. Zhu, and C.-H. Cheng, "Design of ultra-wideband, multi-wideband, and multi-function phase shifters based on multiple resonant technology," in *IEEE MTT-S Int. Microw. Symp. Dig.*, Guangzhou, China, May 2019, pp. 19–22.
[28] X. Guo, L. Zhu, and W. Wu, "Design of complex weighted feeding network based on generalized coupled-resonator filter theory," *IEEE Trans. Microw. Theory Techn.*, vol. 67, no. 11, pp. 4376–4385, Nov. 2019.
[29] H.-R. Ahn and I. Wolff, "General design equations, small-sized impedance transformers, and their applications to small-sized three-port 3-dB power dividers," *IEEE Trans. Microw. Theory Techn.*, vol. 49, no. 7, pp. 1277–1288, Jul. 2001.
[30] S. Zhang and L. Zhu, "Synthesis method for even-order symmetrical Chebyshev bandpass filters with alternative J/K inverters $\lambda/4$ and resonators," *IEEE Trans. Microw. Theory Techn.*, vol. 61, no. 2, pp. 808–816, Feb. 2013.
[31] Y. P. Lyu, L. Zhu, and C.-H. Cheng, "Proposal and synthesis design of differential phase shifters with filtering function," *IEEE Trans. Microw. Theory Techn.*, vol. 65, no. 8, pp. 2906–2917, Aug. 2017.
[32] Y. L. Wu, Z. Zhuang, G. Y. Yan, Y. A. Liu, and Z. Ghassemlooy, "Generalized dual-band unequal filtering power divider with independently controllable bandwidth," *IEEE Trans. Microw. Theory Techn.*, vol. 65, no. 10, pp. 3838–3848, Oct. 2017.
[33] D. Lu, M. Yu, N. S. Barker, M. Li, and S.-W. Tang, "A simple and general method for filtering power divider with frequency-fixed and frequency-tunable fully canonical filtering-response demonstrations," *IEEE Trans. Microw. Theory Techn.*, vol. 67, no. 5, pp. 1812–1825, May 2019.
[34] G. L. Dai, X. Y. Zhang, C. H. Chan, Q. Xue, and M. Y. Xia, "An investigation of open- and short-ended resonators and their applications to bandpass filters," *IEEE Trans. Microw. Theory Techn.*, vol. 57, no. 9, pp. 2203–2210, Sep. 2009.
[35] J.-S. Hong and M. J. Lancaster, *Microstrip Filters for RF/Microwave Application*. New York, NY, USA: Wiley, 2001.

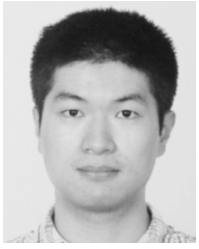

YUN-PENG LYU (S'16–M'18) received the B.Eng. and Ph.D. degrees from the Nanjing University of Posts and Telecommunications (NUPT), Nanjing, China, in 2013 and 2018, respectively.

From 2015 to 2017, he was a Research Assistant with the Department of Electrical and Computer Engineering, University of Macau, China, where he was involved with research. Since 2018, he has been serving as an Assistant Professor with NUPT. His research interests include microwave circuits and antenna theory.

Dr. Lyu is a reviewer for several journals, including the IEEE TRANSACTIONS ON MICROWAVE THEORY AND TECHNIQUES, IEEE TRANSACTIONS ON COMPONENTS, PACKAGING, AND MANUFACTURING TECHNOLOGY, IEEE MICROWAVE AND WIRELESS COMPONENTS LETTERS, *IET Microwaves, Antennas & Propagation*, and *IET Electronics Letters*.

LEI ZHU (S'91–M'93–SM'00–F'12) received the B.Eng. and M.Eng. degrees in radio engineering from the Nanjing Institute of Technology (currently Southeast University), Nanjing, China, in 1985 and 1988, respectively, and the Ph.D. degree in electronic engineering from The University of Electro-Communications, Tokyo, Japan, in 1993.

From 1993 to 1996, he was a Research Engineer with Matsushita-Kotobuki Electronics Industries Ltd., Tokyo. From 1996 to 2000, he was a Research Fellow with the École Polytechnique de Montreal, Montreal, QC, Canada. From 2000 to 2013, he was an Associate Professor with the School of Electrical and Electronic Engineering, Nanyang Technological University, Singapore. In 2013, he joined the Faculty of Science and Technology, University of Macau, Macau, China, as a Full Professor, where he has been a Distinguished Professor, since 2016. From 2014 to 2017, he served as the Head of the Department of Electrical and Computer Engineering, University of Macau. He has authored or coauthored more than 480 articles in international journals and conference proceedings. His articles have been cited more than 6100 times with the H-index of 41 (source: ISI Web of Science). His current research interests include microwave circuits, periodic structures, planar antennas, and computational electromagnetic techniques.

Dr. Zhu served as a member for the IEEE MTT-S Fellow Evaluation Committee, from 2013 to 2015, and has been serving as a member of the IEEE AP-S Fellows Committee, from 2015 to 2017. He was a recipient of the 1997 Asia-Pacific Microwave Prize Award, the 1996 Silver Award of Excellent Invention from Matsushita-Kotobuki Electronics Industries Ltd., and the 1993 First-Order Achievement Award in Science and Technology from the National Education Committee, China. He served as the General Chair for the 2008 IEEE MTT-S International Microwave Workshop Series on the Art of Miniaturizing RF and Microwave Passive Components, Chengdu, China, and the Technical Program Committee Co-Chair of the 2009 Asia-Pacific Microwave Conference, Singapore. He was an Associate Editor of the IEEE TRANSACTIONS ON MICROWAVE THEORY AND TECHNIQUES, from 2010 to 2013, and the IEEE MICROWAVE AND WIRELESS COMPONENTS LETTERS, from 2006 to 2012.

CHONG-HU CHENG (M'01) received the B.S., M.S., and Ph.D. degrees in electronic science and engineering from Southeast University, Nanjing, China, in 1983, 1986, and 1993, respectively. From 1994 to 1996, he was a Postdoctoral Researcher with the Department of Information Electronics, Zhejiang University, China. From 1996 to 1999, he was a Lecturer with Hainan University, China. From 1999 to 2001, he was a Research Fellow with the National Institute of Information and Communications Technology, Japan. He joined the College of Telecommunications and Information Engineering, Nanjing University of Posts and Telecommunications, as an Associate Professor, in 2001, and became a Full Professor, in 2006. He has authored or coauthored more than 100 technical publications. His research interests include computational electromagnetics, small antennas, and microwave passive circuits. He is a member of China Institute of Electronics, Antenna Society. He served as a Reviewer for several international journals, including the IEEE MICROWAVE AND WIRELESS COMPONENTS LETTERS and *IET Electronics Letters*.